Laplace DLTS study of defects introduced in GaAs during sputter deposition of Au Schottky contacts

F. Taghizadeh [*], P.J. Janse van Rensburg, W.E. Meyer, F.D. Auret

Department of Physics, University of Pretoria, Private Bag X20, Hatfield, 0028, Pretoria, South Africa

ABSTRACT

The RF sputter deposition was used to fabricate Au Schottky barrier diodes on Si-doped n-type GaAs with two different carrier densities (1×10^{15} cm^{-3}, 1×10^{16} cm^{-3} and partially 8×10^{16} cm^{-3}) at a power of 150 W. Deep-level transient spectroscopy (DLTS) and Laplace DLTS were used to measure the electrical properties of the sputter-induced defects near the surface of the GaAs. By using DLTS, we found that the samples contained six defects (S1 (0.046 eV), S2 (0.22 eV), S3 (0.30 eV), S4 (0.55 eV), S5 (0.56 eV) and S6 of which three (S1, S3 and S5) were metastable and one (S4) was highly dopant concentration dependent. S6 was observed close to where the EL2 was expected, but had different properties and two components which could be resolved by Laplace DLTS: S6a (0.83 eV) and S6b (0.84 eV). The depth profile showed a difference in depth distribution of the defects in the samples which shows by increasing depth, a rapid decay of defect concentration. The electric field dependence of the S3 defect could be explained by a combination of Poole-Frenkel and phonon-assisted tunnelling mechanisms while for the S4 and S5 defects the emission of carriers indicate the phonon-assisted tunnelling. True capture cross-section measurements were done, and the S3 defect had a much lower capture cross-section than the S4 and S5 defects and the real capture cross-section of S3 and S4 defects is in the range of Auger mechanism while for the S5 defect indicates multiphonon emission. Finally, measurements as to the effect of annealing on *I–V* characteristics were carried out on the sputtered samples as well.

1. Introduction

Sputter deposition is one of the important physical vapour deposition techniques used to deposit thin films onto surfaces [1]. The technique has various advantages such as good adhesion to different substrates, ability to deposit high melting point metals and high deposition rates [2,3]. The sputter deposition is based on bombardment of the target by high energy ions. A gaseous plasma is created and accelerated which then collides with the source material to be deposited (target). These high energy collisions result in ejection of neutral particles from the surface of the target which then travel in a straight line until they either collide with another particle or the surface of the sample [1]. Due to the energetic particles involved in the deposition process, this technique causes damage at the surface and sub-surface of the substrate which includes structural disorder and non-stoichiometry of compound semiconductors. Various defects produced introduce energy levels in the bandgap of the semiconductor [4]. These defects play a significant role in determining the electrical properties of Schottky barrier diodes (SBDs) on these semiconductors. They also reduce the mobility and carrier lifetimes and therefore affect devices such as solar cells and HEMTs relying on these properties fabricated directly below the surface [5,6]. Schottky barrier diodes on sputtered samples have a lower barrier height on n-type material and higher on p-type material when compared to irradiated samples [4,7,8]. Depth profiles show that most of the defects introduced by sputter deposition are close to the surface and by increasing the carrier concentration the depth distribution range is decreased. However, some of these defects may diffuse deeper into the material, influencing structures deeper below the surface. This may be enhanced by conditions such as high temperature or irradiation. It also can be explained that the sputter deposition induced defects which were introduced at the surface drift into the sample due to the electric field effect [7].

Deep-level transient spectroscopy (DLTS) and especially Laplace DLTS (high-resolution DLTS) is one of the powerful techniques used to analyse defects [9,10]. Laplace DLTS has higher resolution compared to conventional DLTS and is capable of separating defects which have similar carrier emission rates [11]. Previous DLTS studies on sputter-deposition induced defects in GaAs have been published [7],

---

however, since their publication, the development of Laplace DLTS has allowed for more detailed and higher resolution analysis. In a previous paper [8] we focused on the *I–V/C–V* measurements, DLTS spectra, Laplace spectra of the S6 defects, Arrhenius plots, and metastability transformation measurements [8]. The current paper presents the depth profiles of the defects, their true capture cross section measurements and the field dependence of the emission rate from the defects.

2. Experimental procedure

Silicon doped (*n*-type) GaAs samples, grown by metal-organic vapour phase epitaxy (MOVPE) on 10^{18} cm^{-3} Si-doped substrates with (100) orientation, were used in this study. Most of the experiments were performed on epitaxial material with carrier densities of 1.0×10^{15} cm^{-3} and 1.0×10^{16} cm^{-3}, while for one experiment, material with a carrier density of 8.0×10^{16} cm^{-3} was used. For ohmic contacts, samples were first degreased in trichloroethylene and isopropanol for 5 min each to remove organic contaminants, then dipped in de-ionized water, and subsequently etched with a solution of H_2O: H_2O_2 [50%]: NH_4OH [25%] with 100:1:3 vol ratio, for 60 s. The final step was the removal of the oxide layer by dipping our samples in a 20% HCl solution for 1 min, then rinsing in de-ionized water, and finally annealing at 450 °C for 2 min in an Ar atmosphere. In this study Ni (5 nm)/Au–Ge (145 nm)/Ni (50 nm) layers were used to make an ohmic contact. For the Schottky contacts, the cleaning procedure was the same as for the ohmics, except that the second step (wet etching) was not included and circular Au contacts, 200 nm thick, were deposited under RF power of 150 W at an Ar pressure of 8.0×10^{-2} mbar with a DC bias of 580 V for 5 min.

The control sample was prepared similarly, except that the Schottky contacts, 1000 Å-thick Au, were deposited using resistive deposition through a 0.6 mm contact mask using the same deposition chamber which was used for the ohmic contacts [8].

The *I–V/C–V* measurements were done at 25 °C, using an HP 4140 B pA Meter/Voltage Source and an HP 4192 LF Impedance Analyser, with the voltage monitored with an HP 34401A multimeter. The electrical properties of the defects were obtained from Laplace DLTS, using a dedicated Laplace DLTS card, and pulse conditions were monitored by an oscilloscope.

3. Results and discussion

Fig. 1 shows the DLTS spectra of the sputter-induced defects in the samples as well as that of a control sample with a 1.0×10^{15} cm^{-3} carrier concentration. The DLTS spectra were obtained in the 20–405 K temperature range at rate window of 80 s^{-1}, by applying a reverse bias of −1 V and a filling pulse amplitude of 1.4 V. The control sample only showed the EL2, while the sputtered sample, when measured while scanning downwards in temperature (curve (b)) displayed six defects (S1, S2, S3, S4, S5 and S6). When scanning upwards in temperature, S4 and S6 were not influenced by the bias the sample was cooled under, however, when the sample was cooled under reverse bias, S5 was not observed (curve (c)) while when cooling under forward bias, the S1 and S3 were not observed (curve (d)). The amplitude of S2 was too small to detect reliably. It was shown that the S3 and S5 defects transformed into each other [8]. Using Laplace DLTS, we found that the S6 defect consisted of two different components (S6a and S6b) [8] we postulate that the S6b, having an amplitude of approximately half that of the S6a, is due to the modification of the EL2 by a nearby defect.

The Arrhenius plots of the seven defects (at 26 K, 140 K, 180 K, 265 K, 320 K and 348 K) in *n*-type GaAs with a carrier concentration of 1.0×10^{15} cm^{-3} are shown in Fig. 2. The activation energies and apparent capture cross section of this study and previous study by Auret et al. [7] are listed in Table 1. As shown in the table, the defects S1, S2, S3 and S4 are similar to the Es1, Es3, Es4 and Es5 reported by Auret et al. The S6a and S6b were not reported by Auret et al. [7], as the authors assumed that the defect was the EL2. These results were discussed in detail in
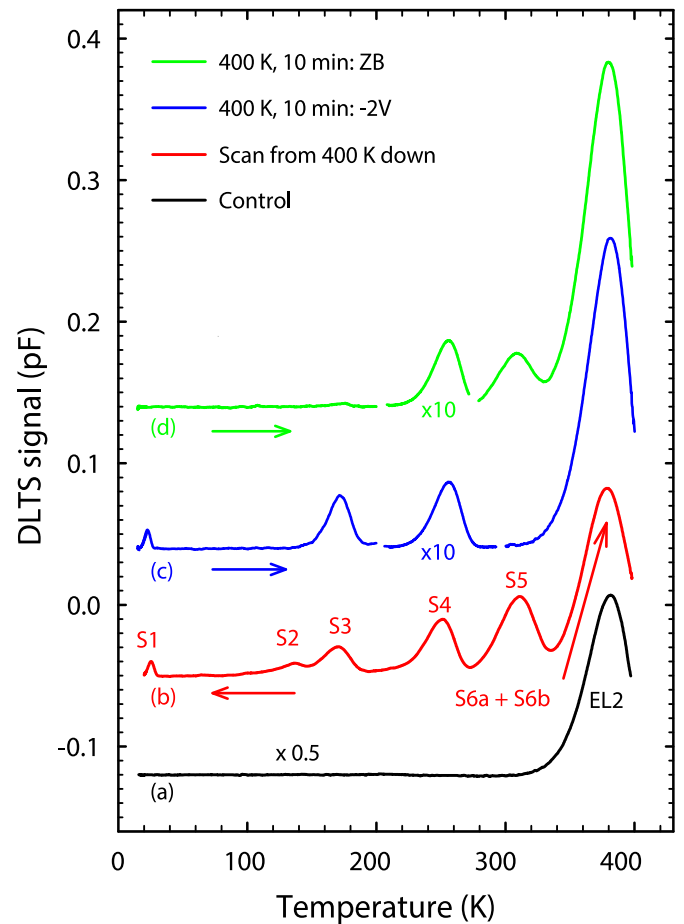

Fig. 1. DLTS spectra of (a) a control sample; (b) a highly doped sample (1.0×10^{16} cm^{-3}) directly after sputtering, scanned downwards in temperature; (c) a lowly doped sputtered sample (1.0×10^{15} cm^{-3}) measured after applying −2 V at 400 K for 10 min, and (d) the same sample measured after applying zero bias for 10 min at 400 K. In the case of (c) and (d), the samples were cooled under the specified bias conditions, and the DLTS spectrum was recorded while scanning upwards in temperature. The reverse bias, V_r, and filling pulse amplitude, V_p, were −1.0 and 1.4 V, respectively, with a 1 ms pulse width, and a rate window of 80 s^{-1} for all samples [8]. The arrows show the direction in which the temperature was scanned.
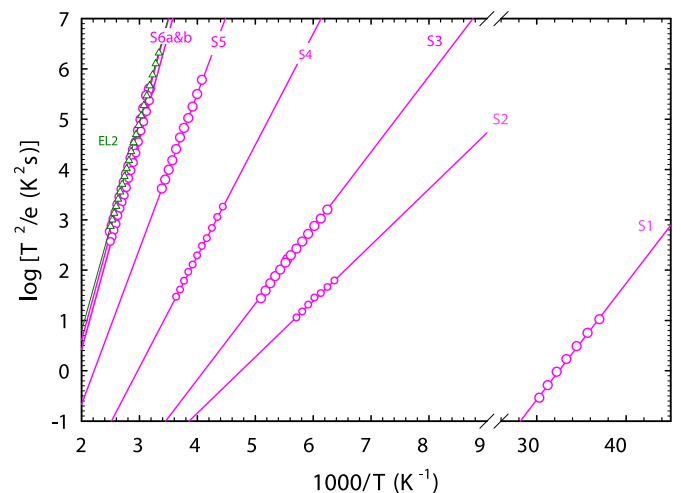

Fig. 2. Arrhenius plots of sputter-deposition induced defects (circles) and the EL2 (triangles), as observed in n-GaAs with carrier density of 10^{15} cm^{-3}.

Table 1

Summery of properties of sputter induced defects (S1 – S6), sputter induced defects (Es1 – Es5) [7] and the EL2.

Defect label	Origin S = sputter N = native	E_A (eV)	σ_a (cm²)	Stability
S1 (this study)	S	0.046	3.1×10^{-13}	Metastable
Es1 [7]	S	0.051	4.3×10^{-14}	–
Es1a [7]	S	0.077	7×10^{-16}	–
S2 (this study)	S	0.22	1.9×10^{-15}	Stable
Es2 [7]	S	0.132	9.1×10^{-14}	
Es2a [7]	S	0.171	1.7×10^{-13}	
Es2b [7]	S	0.211	2.6×10^{-13}	
S3 (this study)	S	0.30	1.6×10^{-14}	Metastable (transformed to S5)
Es3 [7]	S	0.209	4.7×10^{-15}	–
Es3a [7]	S	–	–	–
S4 (this study)	S	0.55	1.0×10^{-12}	Stable
Es4 [7]	S	0.305	9.3×10^{-15}	
Es4a [7]	S	–	–	
Es4b [7]	S	0.438	1.4×10^{-14}	
S5 (this study)	S	0.56	1.3×10^{-14}	Metastable (transformed to S3)
Es5 [7]	S	0.528	2×10^{-13}	–
S6a (this study)	S	0.83	8.8×10^{-13}	Stable
S6b (this study)	S	0.84	6.6×10^{-13}	Stable
EL2	N	0.82	3.2×10^{-13}	Stable

Ref. [8].

The depth profiles of the defects in GaAs with three carrier densities $(1.0 \times 10^{15}$ cm⁻³, 1.0×10^{16} cm⁻³ and 8.0×10^{16} cm⁻³) are shown in Fig. 3. For higher carrier densities, possibly due to the high electric field, the S5 transformed away during the measurement, making accurate measurements impossible. The S5 is therefore only shown for the 1×10^{15} cm³ doped material. The defect depth profiles showed marked differences depending on the carrier densities. In the higher carrier
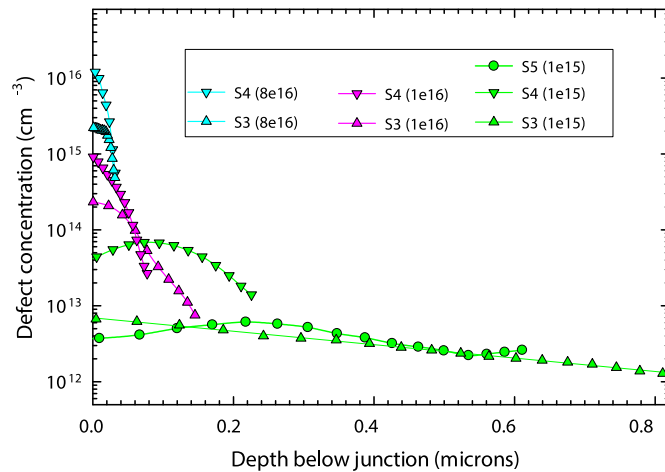
Fig. 3. Depth profiles of the observed deep-level defects in samples with different carrier densities $(1.0 \times 10^{15}$ cm⁻³, 1.0×10^{16} cm⁻³ and 8.0×10^{16} cm⁻³).

density materials, the defect concentrations were higher, but their concentration decayed much faster with increasing depth. This may be due to enhanced diffusion in the depletion region (which in lower doped material is wider), possibly because of the electric field in the depletion region or the charge state of the defects. Another mechanism considered by Ref. [7] is that defects diffuse away from the surface region by recombination enhanced diffusion activated by the electron-hole pairs created by the energetic electrons or the glow discharge during deposition. This should also lead to depth distributions related to the depletion region widths [7].

The electric field dependence of the emission from the sputter-induced defects S3 and S4 was measured in the sample with a 1.0×10^{15} cm⁻³ carrier density in different temperature ranges, with the results shown in Fig. 4. For these measurements, only a narrow depth range of defects are sampled by subtracting two transients measured with different filling pulse levels. The electric field at the depth of the defects is calculated from the depletion approximation. By using a reverse bias in the range 1 V–9 V, a range of fields. According to the Poole-Frenkel model, the log of the emission rate is proportional to the square root of the electric field [12].

$$e(E) = e(0)\exp\left(\frac{1}{kT}\sqrt{\frac{qE}{\pi\varepsilon}}\right) \tag{1}$$

While the phonon-assisted tunnelling mechanism [12] predicts the log of the emission rate to increase as the square of the field

$$e(E) = e(0)\exp\left(\frac{\tau_2^3 e^2 E^2}{3m^*\hbar}\right) \tag{2}$$

In the above equations, $e(0)$ is the emission rate of defect at zero electric field, k is the Boltzmann's constant, T is the temperature, ε is permittivity of semiconductor and E is electric field. Therefore, the log of the emission rate having a linear correlation with $E^{1/2}$ would indicate the Poole-Frenkel mechanism being dominant, while a linear correlation with E^2 would indicate phonon-assisted tunnelling dominating.

For the S3 defect, the emission of carriers was described by phonon-assisted tunnelling at low fields and then changed to Poole-Frenkel at higher fields, with the change occurring at a field of around 1.2×10^9 V/cm. For the S4 defect, the emission of carriers indicated the phonon-assisted tunnelling. Fig. 5 displays the electric field dependence of the S5 defect, and indicates that the emission of carriers for the S5 defect occurred through the phonon-assisted tunnelling mechanism.

For clarity we have summarized coefficients of determination (equal to r² from the graphs) of defects of S3 to S5 in Table 2.

The true capture cross-section measurements of the 1.0×10^{15} cm⁻³ samples for S3, S4 and S5 defects were performed in a different temperature range. All the measurements were done under ($V_r = -2$, $V_{P1} = 0.06$ and $V_{P2} = -1$ V), with different pulse widths at a specific temperature. The DLTS signal after application of a filling pulse of length t_p, can be described by Ref. [13],

$$C(t_p) = C_{inf}\left[1 - exp\left(\frac{-t_p}{\tau_c}\right)\right] \tag{3}$$

where C_{inf} is the magnitude of the DLTS signal where a filling pulse sufficiently long to fill all the defects was applied, and τ_c is the time constant of the capture process given by

$$\tau_c = \sigma N_d v_{th} \tag{4}$$

In this equation σ is the capture cross-section, N_d is the free carrier density and v_{th} is the thermal velocity of the carriers. Accordingly, σ can be calculated from the slope of the plot shown in Fig. 6:

$$\sigma = 2.3 slope/N_D v_{th} \tag{5}$$

Fig. 6 shows the results of the capture cross-section measurements, and shows that the slope increases with increasing temperature. The S3
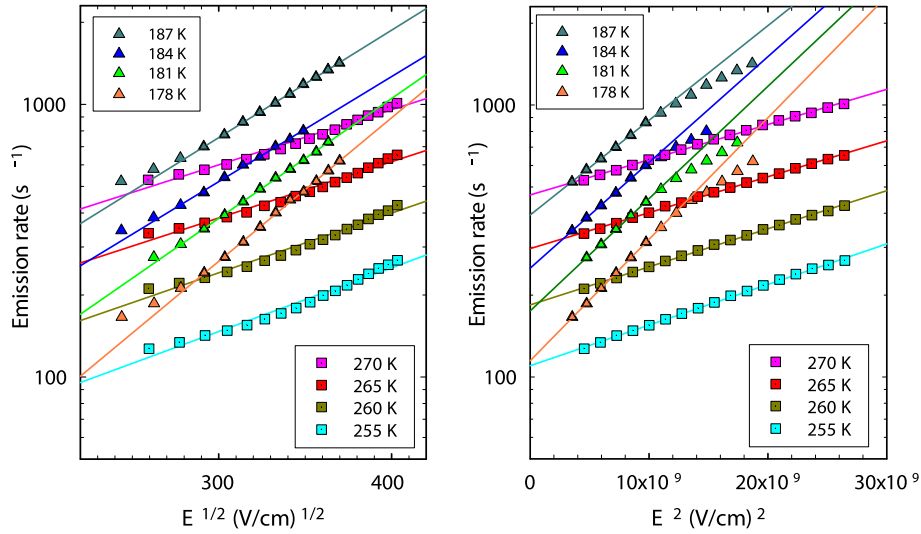
Fig. 4. The electric field dependence of the emission rate of the S3 and S4 defects in the 1.0×10^{15} cm^{-3} doped sample. Note that, in both graphs, the triangle and square symbols relate to the S3 and S4 defects, respectively.
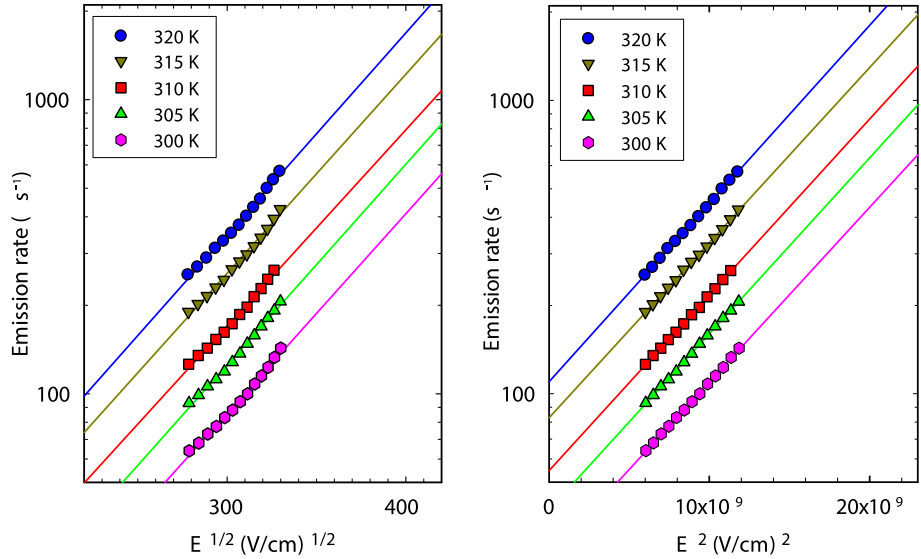
Fig. 5. The electric field dependence of the S5 defect in the 1.0×10^{15} cm^{-3} doped sample.

Table 2
The coefficient of determination of the S3 to S5 defects.

Defects	Coefficient determination of Poole- Frenkel	Coefficient determination of Phonon assisted tunnelling
S3	0.9929–0.99967	0.9996–0.9903
S4	0.9778	0.9988
S5	0.9923	0.9994

defect had a much lower capture cross-section than the other defects (S4 and S5). The real capture cross-section measured for S3, S4 and S5 defects by applying Eqn. (3). are presented in Table 3.

The temperature dependence of the capture cross-section may be explained by the existence of a capture barrier, ΔE, so that the observed capture cross-section as a function of the temperature can be described by

$$\sigma(T) = \sigma_\infty e^{\frac{-\Delta E}{kT}} \qquad (6)$$

Here σ_∞ is the high temperature limit of the capture cross-section, k

is the Boltzmann constant and T is the temperature. As seen in Table 3, the capture cross-sections for S3, S4 and S5 defects were measured at different temperatures and used in Fig. 7 to calculate the capture barriers. As shown in Fig. 7, the capture barriers for these defects are 0.05 eV (S3), 0.09 eV (S4) and 0.50 eV (S5). The high temperature limit of capture cross-section (σ_∞) for S3, S4 and S5 were calculated to be (1.98 $\times 10^{-17}$ cm^2, 1.06 $\times 10^{-16}$ cm^2 and 4.33 $\times 10^{-9}$ cm^2, respectively).

As mentioned in Table 3, the real capture cross-sections for S3 and S4 defects are of the order of 10^{-19} cm^2 and 10^{-18} cm^2, which is in the range of the Auger mechanism, according to Henry et al. [14]. But the S5 defect's capture cross-section is of the order of 10^{-17} cm^2, which is strongly exponential temperature dependent ($\Delta E = 0.50$). This feature indicates that this capture occurs through multiphonon emission (MPE) [15,16].

Fig. 8 (a) and (b) display the effect of annealing temperature on ideality factor and series resistance of the 1.0×10^{15} cm^{-3} and 1.0×10^{16} cm^{-3} doped sputtered materials. We annealed these samples under vacuum isochronally for 10 min, starting at a 425 K and increasing in 25 K steps. As seen in Fig. 8 (a), the ideality factor for the 1.0×10^{15} cm^{-3}
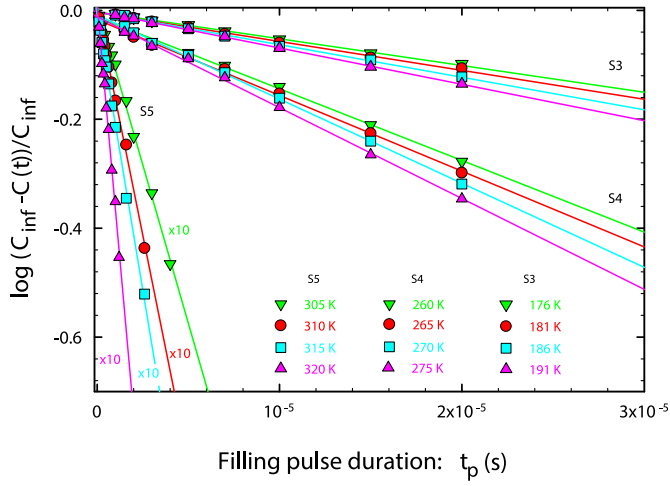
Fig. 6. Determination of the capture cross-sections of the S3, S4 and S5 defects in GaAs for the 1.0×10^{15} cm^{-3} doped sample.
[Note: all the data points for the S5 defects have been multiplied by 10 as indicated in the figure].

Table 3
The capture cross-sections of the S3, S4 and S5 defects at different temperatures.

Defect	Temperature (K)	σ_n (cm^2)
	176	6.43×10^{-19}
S3	181	6.84×10^{-19}
	186	7.62×10^{-19}
	191	8.38×10^{-19}
	260	1.39×10^{-18}
S4	265	1.49×10^{-18}
	270	1.67×10^{-18}
	275	1.74×10^{-18}
	305	1.81×10^{-17}
S5	310	2.78×10^{-17}
	315	3.32×10^{-17}
	320	4.90×10^{-17}
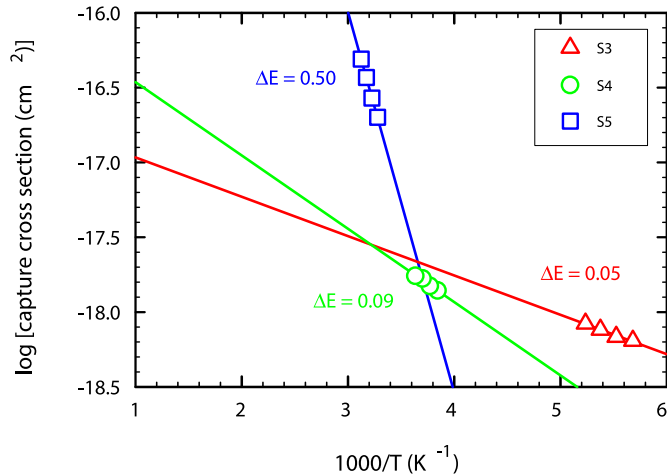
Fig. 7. Arrhenius plots for the determination of the capture barriers of the S3, S4 and S5 defects in GaAs with a doping density of 1.9×10^{15} cm^{-3}.

doped sample improved gradually with annealing, however, it increased significantly at 725 K. In contrast, the ideality factor of the 1.0×10^{16} cm^{-3} doped sample was almost constant and it started to increase after annealing above 575 K. These results may be explained by the highly doped material having a high concentration of defects close to the interface (as shown in Fig. 3), leading to faster degradation of the
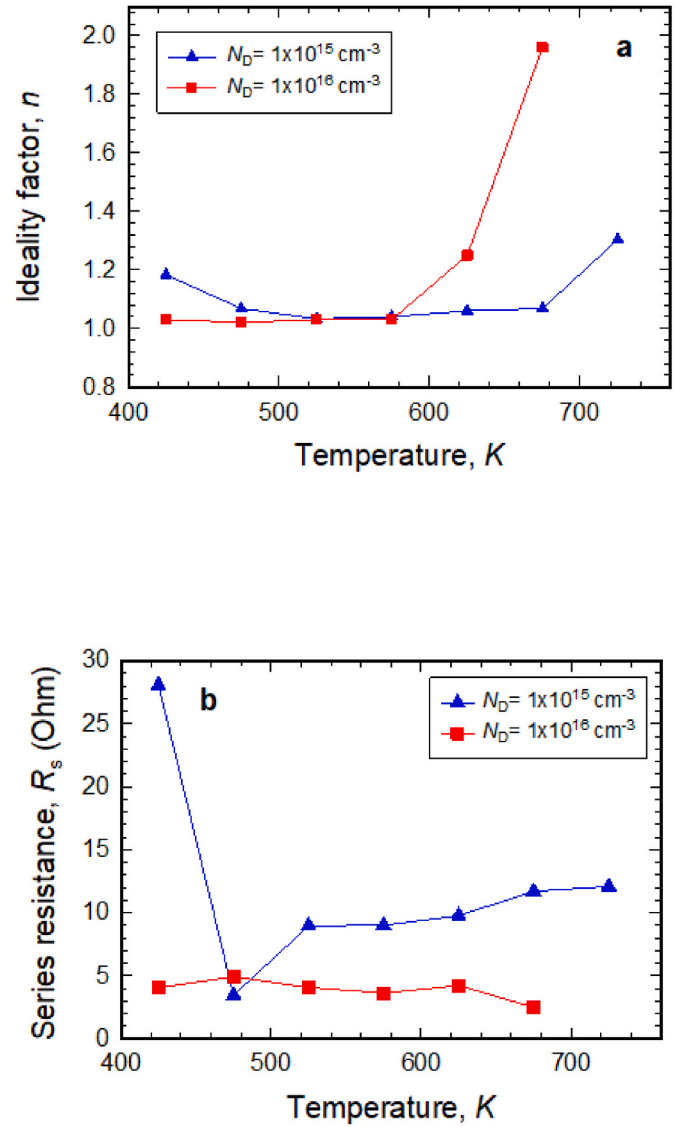
Fig. 8. The (a) ideality factor and (b) series resistance after annealing for the 1.0×10^{15} cm^{-3} and 1.0×10^{16} cm^{-3} doped samples.

Schottky diode.

Fig. 8 (b) shows the series resistance vs annealing temperature. For the lower doped material (1.0×10^{15} cm^{-3}) sample, the series decreased sharply and then increased slowly with increasing annealing temperatures, but for the 1.0×10^{16} cm^{-3} doped sample, the series resistance decreased only insignificantly with increasing annealing temperature. The difference may be due to the resistivity of the lower carrier density material being more sensitive to the presence of defects.

4. Conclusion

Au Schottky barrier diodes on Si-doped n-type GaAs for three different carrier densities (1×10^{15} cm^{-3}, 1×10^{16} cm^{-3} and 8×10^{16} cm^{-3}) fabricated by using RF sputter deposition at a power of 150 W were characterized. Laplace DLTS was used to measure the electrical properties of the sputter-induced defects on GaAs. These defects are (S1 (0.046 eV), S2 (0.22 eV), S3 (0.30 eV), S4 (0.55 eV), S5 (0.56 eV) and S6a (0.83 eV) and S6b (0.84 eV)). The depth profile results illustrated that the lower doped material (1.0×10^{15} cm^{-3}) had deeper defects with a lower concentration under the Schottky junction compared to the higher carrier density material, which can be explained by enhanced

diffusion in the depletion region. The S4 defect was closer to the surface compared to the S3 and S5 defects. The electric field enhanced emission from defects was measured for S3, S4 and S5 defects, and the emission of carriers of S3 defect was a combination of the phonon-assisted tunnelling and the Poole-Frenkel effect, while for the S4 and S5 defects the emission of the carriers occurs through phonon-assisted tunnelling. The capture cross-sections of these defects were measured and the S5 defect has a larger capture cross-section compared to the other defects. In addition, the capture barrier and high temperature limits of the capture cross-section were measured, and the results for the S5 defect were found to be higher. The capture cross-section values for the S5 defect can be explained by the multiphonon emission (MPE) mechanism and for the S3 and S4 defects they agree with the Auger mechanism. By increasing the annealing temperature, the ideality factor initially improved for 1.0×10^{15} cm^{-3}, but for 1.0×10^{16} cm^{-3} sample it was almost constant up to 575 K, where after it started to increase.

The series resistance for the 1.0×10^{15} cm^{-3} doped sample decreased significantly at first, then increased with increasing annealing temperature, whereas a much smaller change was shown for the 1.0×10^{16} cm^{-3} doped sample.

Authorship statement

All persons who meet authorship criteria are listed as authors, and all authors certify that they have participated sufficiently in the work to take public responsibility for the content, including participation in the concept, design, analysis, writing, or revision of the manuscript. Furthermore, each author certifies that this material or similar material has not been and will not be submitted to or published in any other publication before its appearance in the *Hong Kong Journal of Occupational Therapy*.

Please indicate the specific contributions made by each author (list the authors' initials followed by their surnames, e.g., Y.L. Cheung). The name of each author must appear at least once in each of the three categories below.

Category 1.

Conception and design of study: F. Taghizadeh, F.D. Auret,

Acquisition of data: F. Taghizadeh, F.D. Auret,

Analysis and/or interpretation of data: F. Taghizadeh, F.D. Auret, W. E. Meyer, P.J. Janse van Rensburg.

Category 2.

Drafting the manuscript: F. Taghizadeh, F.D. Auret,

Revising the manuscript critically for important intellectual content: F.D. Auret, W.E. Meyer, P.J. Janse van rensburg.

Category 3.

Approval of the version of the manuscript to be published (the names of all authors must be listed):

F. Taghizadeh, F.D. Auret, W.E. Meyer, P.J. Janse van Rensburg.

CRediT authorship contribution statement

F. Taghizadeh: Writing – review & editing, Writing – original draft, Visualization, Validation, Methodology, Investigation, Formal analysis, Data curation, Conceptualization. **P.J. Janse van Rensburg:** Writing – review & editing, Methodology, Formal analysis. **W.E. Meyer:** Writing – review & editing, Supervision, Funding acquisition, Formal analysis. **F. D. Auret:** Writing – review & editing, Visualization, Supervision, Methodology, Investigation, Funding acquisition, Formal analysis, Data curation, Conceptualization.

Declaration of competing interest

The authors declare the following financial interests/personal relationships which may be considered as potential competing interests: Fatemeh Taghizadeh reports financial support was provided by University of Pretoria. Fatemeh Taghizadeh reports a relationship with

University of Pretoria that includes: funding grants.

Data availability

No data was used for the research described in the article.

References

[1] D. Depla, S. Mahieu, J.E. Greene, Sputter deposition processes, in: Handbook of Deposition Technologies for Films and Coatings, Elsevier Inc., 2010, pp. 253–296.
[2] Y. Leclerc, F.D. Auret, S.A. Goodman, G. Myburg, C. Schutte, Electronic properties of defects introduced during sputter deposition of Cr Schottky contacts on GaAs, in: Ion Beam Modification of Materials, Elsevier, 1996, pp. 870–873.
[3] F.D. Auret, S.A. Goodman, G. Myburg, W.O. Barnard, Electrical characterization of sputter-deposition-induced defects in epitaxially grown n-GaAs layers, Vacuum 46 (8–10) (Aug. 1995) 1087–1090, https://doi.org/10.1016/0042-207X(95)00112-3.
[4] F.D. Auret, S.A. Goodman, G. Myburg, W.E. Meyer, Electrical characteristics of Ar-ion sputter induced defects in epitaxially grown n-GaAs, J. Vac. Sci. Technol. B Microelectron. Nanom. Struct. 10 (6) (Nov. 1992) 2366, https://doi.org/10.1116/1.586069.
[5] R. Tang, et al., Controlled sputtering pressure on high-quality Sb2Se3 thin film for substrate configurated solar cells, Nanomaterials 10 (3) (Mar. 2020) 574, https://doi.org/10.3390/nano10030574.
[6] R.E. Thomas, Solar Energy Conversion, Elsevier, 1979.
[7] F.D. Auret, S.A. Goodman, Y. Leclerc, G. Myburg, C. Schutte, Electronic properties of defects introduced in GaAs during sputter deposition of gold Schottky contacts, Mater. Sci. Technol. 13 (11) (1997) 945–948, https://doi.org/10.1179/mst.1997.13.11.945.
[8] F. Taghizadeh, P.J. Janse van Rensburg, K. Ostvar, W.E. Meyer, F.D. Auret, Electronic properties and transformation kinetics of two prominent metastable defects introduced in GaAs during sputter deposition of Au Schottky contacts, Mater. Sci. Semicond. Process. 99 (Aug. 2019) 23–27, https://doi.org/10.1016/J.MSSP.2019.04.012.
[9] M.G. Lupo, A. Cola, L. Vasanelli, A. Valentini, Deep level transient spectroscopy of Mo/GaAs Schottky barriers prepared by DC sputtering, Phys. Status Solidi 124 (2) (Apr. 1991) 473–481, https://doi.org/10.1002/pssa.2211240212.
[10] D.A. Vandenbroucke, R.L. Van Meirhaeghe, W.H. Laflère, F. Cardon, Sputter-induced damage in Al/n-GaAs and Al/p-GaAs Schottky barriers, Semicond. Sci. Technol. 2 (5) (May 1987) 293–298, https://doi.org/10.1088/0268-1242/2/5/008.
[11] L. Dobaczewski, A.R. Peaker, K. Bonde Nielsen, Laplace-transform deep-level spectroscopy: the technique and its applications to the study of point defects in semiconductors, J. Appl. Phys. 96 (9) (2004) 4689–4728, https://doi.org/10.1063/1.1794997.
[12] S. Ganichev, E. Ziemann, W. Prettl, I. Yassievich, Distinction between the Poole-Frenkel and tunneling models of electric-field-stimulated carrier emission from deep levels in semiconductors, Phys. Rev. B Condens. Matter 61 (15) (Apr. 2000) 10361–10365, https://doi.org/10.1103/PhysRevB.61.10361.
[13] A. Telia, B. Lepley, C. Michel, Experimental analysis of temperature dependence of deep-level capture cross-section properties at the Au oxidized InP interface, J. Appl. Phys. 69 (10) (May 1991) 7159–7165, https://doi.org/10.1063/1.347607.
[14] C.H. Henry, D.V. Lang, Nonradiative capture and recombination by multiphonon emission in GaAs and GaP, Phys. Rev. B 15 (2) (Jan. 1977) 989–1016, https://doi.org/10.1103/PhysRevB.15.989.
[15] A. Mitonneau, A. Mircea, G.M. Martin, D. Pons, Electron and hole capture cross-sections at deep centers in gallium arsenide, Rev. Phys. Appl. 14 (10) (Oct. 1979) 853–861, https://doi.org/10.1051/rphysap:019790014010085300.
[16] D.V. Lang, R.A. Logan, A study of deep levels in GaAs by capacitance spectroscopy, J. Electron. Mater. 4 (5) (Oct. 1975) 1053–1066, https://doi.org/10.1007/BF02660189.